Spontaneous symmetry breaking in coupled parametrically driven waveguides

Nir Dror and Boris A. Malomed
Department of Physical Electronics, School of Electrical Engineering, Faculty of Engineering, Tel Aviv University, Tel Aviv 69978, Israel

(Received 4 September 2008; published 16 January 2009)

We introduce a system of linearly coupled parametrically driven damped nonlinear Schrödinger equations, which models a laser based on a nonlinear dual-core waveguide with parametric amplification symmetrically applied to both cores. The model may also be realized in terms of parallel ferromagnetic films, in which the parametric gain is provided by an external field. We analyze spontaneous symmetry breaking (SSB) of fundamental and multiple solitons in this system, which was not studied systematically before in linearly coupled dissipative systems with intrinsic nonlinearity. For fundamental solitons, the analysis reveals three distinct SSB scenarios. Unlike the standard dual-core-fiber model, the present system gives rise to a vast *bistability* region, which may be relevant to applications. Other noteworthy findings are *restabilization* of the symmetric soliton after it was destabilized by the SSB bifurcation, and the existence of a generic situation with all solitons unstable in the single-component (decoupled) model, while both symmetric and asymmetric solitons may be stable in the coupled system. The stability of the asymmetric solitons is identified via direct simulations, while for symmetric and antisymmetric ones the stability is verified too through the computation of stability eigenvalues, families of antisymmetric solitons being entirely unstable. In this way, full stability maps for the symmetric solitons are produced. We also investigate the SSB bifurcation of two-soliton bound states (it breaks the symmetry between the two components, while the two peaks in the shape of the soliton remain mutually symmetric). The family of the asymmetric double-peak states may decouple from its symmetric counterpart, being no longer connected to it by the bifurcation, with a large portion of the asymmetric family remaining stable.

DOI: 10.1103/PhysRevE.79.016605 PACS number(s): 05.45.Yv, 42.65.Tg, 42.65.Yj, 05.45.Xt

I. INTRODUCTION AND THE MODEL

It is well-known that the balance between gain and loss may support stable solitary pulses (usually referred to as "solitons" in physics literature) in various nonlinear media. This is a vast field of fundamental research [1], which also finds applications of paramount practical significance, as concerns the stabilization of *return-to-zero* pulses in fiber-optic telecommunication networks [2]. An obvious condition necessary for the stability of localized states is the stability of the zero solution, which rules out the simplest models, such as the cubic complex Ginzburg-Landau (CGL) equation with the linear gain [1]. One possibility to create stable pulses is to use linear amplifiers combined with saturable absorbers (in terms of fiber lasers), which leads to the model based on the cubic-quintic CGL equation [3]. Actually, soliton solutions of this equation were investigated in some detail prior to the derivation of the respective fiber-laser models [4]. Other physically relevant equations, which originate in models of fiber lasers based on dual-core fibers (DCFs), with the combination of the linear gain in an active core and loss in a stabilizing one linearly coupled to it, also support stable solitary pulses (see original works [5–8] and review [9]). In the basic version of the latter model, stable dissipative solitons can be found in an exact analytical form [6].

A model of a different type makes it possible to produce a stable soliton supported by the balance of the linear loss (with coefficient $\gamma>0$), linear *parametric gain* (of strength h), and linear *mismatch* q (a wave-number shift between the carrier wave and the spectrum point corresponding to the maximum parametric gain), within the framework of the single nonlinear Schrödinger (NLS) equation [10–12]:

$$i\psi_z - q\psi + (1/2)\psi_{tt} + |\psi|^2\psi = -i\gamma\psi + h\psi^*. \tag{1}$$

This equation is written in terms of fiber optics, where z is the propagation distance, $t=T-z/V_{\rm gr}$ the reduced time (T is usual time, and $V_{\rm gr}$ the group velocity of the carrier wave [2]), ψ the local amplitude of the electromagnetic wave, and the group-velocity dispersion (GVD) is assumed to be anomalous, as usual [2]. In Eq. (1), the effective GVD and Kerr-nonlinearity coefficients are normalized to be 1, and the asterisk stands for the complex conjugation, in the gain term. The parametric gain in telecommunication links [13,14] and laser cavities [15] can be induced, through the nonlinear phase-conjugation mechanism, by amplifiers using a co-propagating pump wave. The gain coefficient in Eq. (1) may be fixed to be real and positive, $h>0$. In addition to the interpretation in terms of fibers, Eq. (1) may also be realized as a model of a planar optical waveguide, with t replaced by transverse coordinate x, and the second-derivative term accounting for the diffraction, in the ordinary paraxial approximation.

The same model applies to easy-axis and easy-plane ferromagnetic media near the Curie point [16,17], where the parametric drive is provided by an external magnetic [18] or microwave [10] field. In that case, ψ in Eq. (1) is the local amplitude of the magnon field, with z and t replaced by time and the spatial coordinate, respectively. Related models with the parametric gain (and, possibly, with additional terms accounting for nonlinear and diffusion losses [19]) are known in other physical contexts, such as waves in nematic and cholesteric liquid crystals in rotating magnetic fields [20], the nonlinear Faraday resonance in vertically vibrating layers of

water [21] or granular materials [22], and commensurate-incommensurate transitions in convective systems [23].

A well-known fact is that Eq. (1) gives rise to two exact soliton solutions [10],

$$\psi_{\pm}(t) = \eta_{\pm} \exp(-i\theta_{\pm})\mathrm{sech}(\eta_{\pm}t),$$

$$2\theta_{+} = \sin^{-1}(\gamma/h), \quad 2\theta_{-} = \pi - \sin^{-1}(\gamma/h),$$

$$\eta_{\pm}^2 = 2(q \pm \sqrt{h^2 - \gamma^2}), \tag{2}$$

provided that $h > \gamma$. Necessary stability conditions for solution ψ_{+} are

$$\gamma < h < \sqrt{q^2 + \gamma^2} \quad \text{and} \quad q > 0, \tag{3}$$

while soliton ψ_{-}, with the smaller amplitude, is always unstable. Full stability conditions for ψ_{+} were reported in Ref. [10] (see also Fig. 10 below). Taking into regard that q must be positive in the model which is going to generate stable solitons, an additional rescaling of Eq. (1) allows one to fix $q \equiv 1$, keeping two free parameters in the model, h and γ.

The objective of the present work is to introduce a system modeling a symmetric DCF, with the parametric gain provided in each core. This setting is a natural extension of the above-mentioned fiber-laser models, which opens a way to enhance the functionality of the laser settings, using effects of the *spontaneous symmetry breaking* (SSB), which were previously studied in terms of continuous waves [24] and temporal solitons in lossless DCFs [25–28], as well as in twin-core fiber gratings [29]. Thus we will be using a system of two equations similar to Eq. (1), with the linear coupling between them, accounted for by an additional coefficient, λ, that may be fixed to be positive too:

$$i\psi_z - \psi + (1/2)\psi_{tt} + |\psi|^2\psi + \lambda\phi = -i\gamma\psi + h\psi^*,$$

$$i\phi_z - \phi + (1/2)\phi_{tt} + |\phi|^2\phi + \lambda\psi = -i\gamma\phi + h\phi^*, \tag{4}$$

ψ and ϕ being the amplitudes of electromagnetic waves in the two cores [as said above, the mismatch parameter is fixed here to be $q \equiv 1$, cf. Eq. (1)].

Equations (4) with t replaced by x also apply to the description of a dual-core planar optical waveguide, with the parametric gain for stationary waves induced in both cores. In addition to the realizations of the coupled system in optics, it can be interpreted too in terms of ferromagnetic media, assuming two parallel easy-axis or easy-plane films, in which the linear coupling is mediated by the intrinsic magnetic field.

The paper is organized as follows. In Sec. II, we produce basic types of bifurcation diagrams which describe the SSB in the model based on coupled equations (4). A vast variety of branches of localized solutions has been found in the system, but a majority of them are completely unstable. With the aim to report physically relevant results, we display only those branches which may be stable, or those completely unstable ones which are involved in bifurcations accounting for destabilization or *restabilization* of other solutions. Taking into regard different stability scenarios, we identify three distinct types of bifurcation diagrams, their noteworthy peculiarity being the presence of a *bistability*: in a parameter region of a conspicuous size, two branches of asymmetric solitons, which are mirror images of each other, and the symmetric soliton may be stable *simultaneously*. The bistability was the original incentive in the works which introduced the concept of the nonlinear optical coupler [30]. This feature is of obvious interest to potential applications, such as all-optical switching (for short pulses in DCFs, switching was demonstrated in experiments [31]). The bistability of solitons in the damped system with the parametric gain is a novel property, as it is, by definition, impossible in the single parametrically driven NLS equation (1), while in the ordinary DCF model, which is based on Eqs. (4) with $\gamma = h = 0$, a bistability is possible, but in a very narrow region, and it has a completely different character [28]. In another context, bistability of solitary pulses in dissipative media was recently reported in systems of linearly coupled CGL equations with the cubic-quintic nonlinearity [32]. In Sec. II we also report another dynamical regime that was not reported before, *viz.*, intrinsic destabilization of asymmetric solitons in the weakly coupled system. The destabilization neither destroys the asymmetric solitons nor restores their symmetry, but rather converts them into robust asymmetric breathers. In the region of weak coupling, the symmetric solitons also get destabilized and turn into robust breathers (which remain symmetric states—in fact, they are tantamount to breathing modes in the single-component model reported in Ref. [10]). As a result, we discover a generic situation with all stationary solitons unstable in the limit of the decoupled (single-component) model, while both symmetric and asymmetric solitons may be stable in the presence of the coupling. In this work, the stability of asymmetric states is analyzed by means of direct simulations of the evolution of perturbed solitons, while for symmetric states this is also done in a more rigorous way, through the computation of eigenvalues for modes of small perturbations around the solitons.

In Sec. III, we additionally analyze the stability of symmetric solitons and identify several types of their stability charts in the parameter space, which turn out to be different from their counterparts in the single-component model [10,11], even if solutions for stationary symmetric solitons are, obviously, the same as in that model. In Sec. IV, which deals with bound states of fundamental solitons, we find a branch of stable asymmetric two-soliton modes bifurcating from the symmetric one. In a certain parameter region, the family of asymmetric bound states exists independently, without a bifurcation linking it to the symmetric counterpart. The paper is concluded by Sec. V.

II. BIFURCATION DIAGRAMS FOR STABLE SOLITONS

A. Preliminaries

Before considering solitons solutions to Eqs. (4) and their stability, it is necessary to analyze the stability of the zero solution, within the framework of the linearized version of these equations, as it is, obviously, a necessary condition for the stability of any localized mode. The analysis is straightforward, and the result is simple: if $\lambda > 1$ [without imposing normalization $q \equiv 1$ onto the mismatch parameter, this con-

dition would be $\lambda > q$, cf. Eq. (1)], the zero solution is stable only for $\gamma > h$, which simply means that the loss coefficient must exceed the gain. Actually, for $\gamma > h$ (regardless of the relation between λ and q) the zero solution is not only stable, but also represents the only attractor in the system, as solitons cannot exist unless h exceeds γ, see Eqs. (2). On the other hand, if the linear coupling is not too strong, i.e., $\lambda < 1$, the full set of stability conditions for the zero solution is

$$h < \sqrt{\gamma^2 + (1-\lambda)^2}, \quad \text{and} \quad 1 - \lambda > 0, \tag{5}$$

cf. necessary stability conditions (3) for soliton ψ_+ in the single parametrically driven NLS equation.

Another elementary but important property of the system of coupled equations (4) is the fact that all its stationary solutions with constant phases, i.e.,

$$\{\psi(t), \phi(t)\} = \{e^{i\Psi} f(t), e^{i\Phi} g(t)\}, \tag{6}$$

with real functions $f(t)$ and $g(t)$ and real constants Ψ and Φ, can be related to stationary solutions of the standard (conservative) model of the nonlinear DCF, i.e., Eqs. (4) with $\gamma = h = 0$. Indeed, a straightforward analysis of the stationary (z-independent) setting demonstrates that any real solution $\{\hat{\psi}(t;\lambda), \hat{\phi}(t;\lambda)\}$ to the system of equations (4) with $h = \gamma = 0$, which contains the single free parameter, λ, generates two stationary solutions to the full system (4) in the following form:

$$\begin{Bmatrix} \psi_\pm(t) \\ \phi_\pm(t) \end{Bmatrix} = (1 \pm \sqrt{h^2 - \gamma^2})^{1/2} e^{-i\theta_\pm} \times \begin{Bmatrix} \hat{\psi}\left((1 \pm \sqrt{h^2 - \gamma^2})^{1/2} t; \dfrac{\lambda}{1 \pm \sqrt{h^2 - \gamma^2}} \right) \\ \hat{\phi}\left((1 \pm \sqrt{h^2 - \gamma^2})^{1/2} t; \dfrac{\lambda}{1 \pm \sqrt{h^2 - \gamma^2}} \right) \end{Bmatrix}, \tag{7}$$

where $\theta_\pm$ are the same constant phases as in the single-component solution (2). Inversely, the stationary solution to full equations can be reduced to the form of Eqs. (7), assuming that the phases of the solution are constant.

In particular, symmetric and antisymmetric solitons in the present model are generated by their commonly known counterparts in the standard DCF model [25,27,28], via Eq. (7):

$$\psi_\pm(t;\lambda) = \sigma \phi_\pm(t;\lambda) = [2(1 \pm \sqrt{h^2 - \gamma^2} - \sigma\lambda)]^{1/2} \times e^{-i\theta_\pm} \operatorname{sech}\{[2(1 \pm \sqrt{h^2 - \gamma^2} - \sigma\lambda)]^{1/2} t\}, \tag{8}$$

where $\sigma = +1$ for symmetric, and -1 for antisymmetric solutions [this sign is independent from $\pm$ in Eq. (8)]. Stable asymmetric solutions of the standard DCF model are generated by the SSB bifurcation from symmetric ones [27,28]. An exact analytical form of those solutions is not available, although they may be accurately represented by means of the variational approximation [26,28,33] (in the case of the weak linear coupling, the perturbation theory for solitons can also be applied to the standard DCF model [34]). The asymmetry of stationary solutions is measured by the parameter

$$\Theta \equiv \frac{E_\psi - E_\phi}{E_\psi + E_\phi}, \quad E_{\psi,\phi} \equiv \int_{-\infty}^{+\infty} |\psi(t), \phi(t)|^2 dt, \tag{9}$$

which is expressed in terms of energies $E_{\psi,\phi}$ of the two components, and total energy $E \equiv E_\psi + E_\phi$. In particular, expression (8) yields the energy of the symmetric and antisymmetric solitons,

$$(E_\sigma)_\pm = 4[2(1 \pm \sqrt{h^2 - \gamma^2} - \sigma\lambda)]^{1/2}. \tag{10}$$

In the standard DCF model, the SSB diagram is represented by plots of Θ versus E. However, the situation in the dissipative system is different, as, for given parameters of Eq. (4), there may exist a single stable solution—or two solutions, in the case of bistability—which are *attractors* of this system, while in the conservative DCF model E is an intrinsic parameter of the continuous soliton family. Thus, for given gain and loss parameters, h and γ, relevant solution families may be adequately represented by pairs of diagrams, one showing $E(\lambda)$, and the other - $\Theta(\lambda)$, for various soliton families that may be stable, or those which are related to stable solutions by bifurcations. This form of the presentation of the results stresses the novelty of the system in comparison with the single-component model based on Eq. (1), where the coupling parameter, λ, does not exist. It is true that, due to relations (7), the set of data representing constant-phase solutions in these diagrams is, as a matter of fact, generated by the standard DCF model, even if the SSB diagram was not presented in the same form in the latter model. However, it will be seen that the stability picture in the present system, i.e., the most significant part of the diagrams, is completely different from that in its DCF counterpart. In particular, while the SSB bifurcation in the DCF model is known to be (slightly) subcritical [28], i.e., the respective asymmetric solitons emerge as unstable modes, in the present system the bifurcation is supercritical, immediately giving rise to stable asymmetric states. Besides that, the diagram will include an additional branch of asymmetric solutions with variable phases (*branch C*, see below), which is absent in the DCF setting. By itself, branch C is always unstable; however, it is a physically significant solution because it provides for *restabilization* of unstable symmetric solitons. It is also worthy to note that, in one of the generic situations reported below, all solitons are unstable in the limit of the decoupled system, i.e., in the single-component NLS equation (1), while the coupled system (4) reveals a large stability region for both symmetric and asymmetric solitons.

B. Diagrams and soliton dynamics. Case 1: a stable pitchfork bifurcation

As said above, symmetric and antisymmetric stationary soliton solutions to Eqs. (4) are given, in the analytical form, by Eqs. (7) and (8). As concerns asymmetric constant-phase solutions, we first found asymmetric solitons of the DCF variant of the model, with $h = \gamma = 0$, by means of the Newton-Raphson method for the solution of the nonlinear boundary-value problem, and then asymmetric localized solutions to the stationary version of Eqs. (4) were generated by means of relations (7). Stability of various solutions was identified

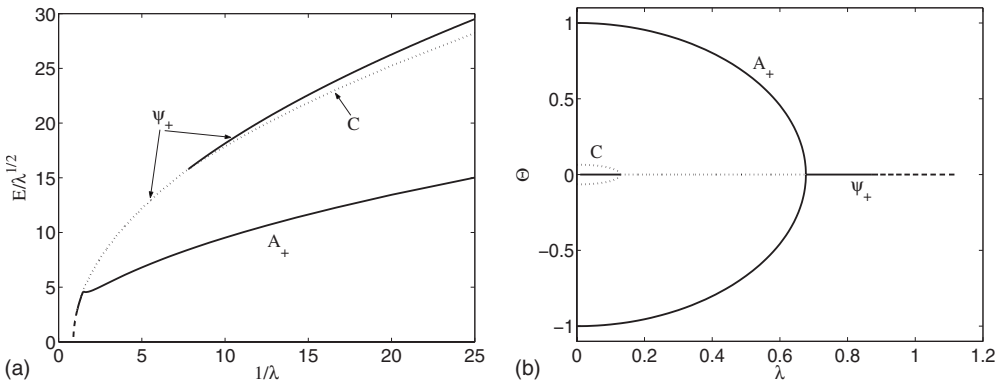

FIG. 1. (a) A set of plots showing the energy of solitons versus inverse coupling constant $1/\lambda$ for symmetric and asymmetric solitons, as well as for the family of unstable asymmetric modes C ("chirped"), the latter one accounting for the bifurcation which *restabilizes* the symmetric solitons. (b) The symmetry-breaking diagram, showing the asymmetry degree of solitons, which is defined as per Eq. (9), versus λ. These diagrams are plotted for $h=0.42$ and $\gamma=0.40$. Here and in other bifurcation diagrams, stable solutions are depicted by continuous lines, while dashed, dotted, and dashed-dotted ones depict three different species of unstable solutions, see the text. Numerous families of completely unstable solitons (in particular, antisymmetric ones), which are not related by bifurcations to branches that may be stable, are not shown (here and below).

through direct simulations of the evolution of perturbed solitons. The simulations were chiefly performed by means of the standard pseudospectral split-step method. In addition, we also used a finite-difference (Crank-Nicolson) algorithm, making use of recipes given in Ref. [35], to check the accuracy of the numerical results produced by the split-step code. In all cases, both simulation methods produced identical results.

The stability of symmetric and antisymmetric solitons was also independently analyzed through the linearization of Eqs. (4) for small perturbations and computation of respective stability eigenvalues. Stability regions for the symmetric solitons found from direct simulations (see below), as well as the fact that all antisymmetric solitons are always unstable, were exactly corroborated by the computation of the eigenvalues. Note that antisymmetric solitons have a small stability region in the ordinary DCF model [27], which completely disappears in the present system.

The results can be summarized by means of a set of bifurcation and stability diagrams that reveal three essentially different situations. The diagrams presented here do not display numerous completely unstable solution branches, unless they are linked to (partly) stable solution families by bifurcations. In particular, all antisymmetric solitons and solutions bifurcating from them are entirely unstable, as well as symmetric solution ψ_-, which is given by Eq. (8) with the lower sign and $\sigma=+1$, and asymmetric modes bifurcating from ψ_-.

The most straightforward scenario which is possible as a generic one is illustrated by the diagrams displayed in Fig. 1, for $h=0.42$ and $\gamma=0.40$. In this figure, and in other bifurcation diagrams displayed below, solid lines depict families of stable solutions, dashed lines are reserved for solutions unstable due to the instability of the zero background [see Eq. (12) below], dotted lines represent solution branches whose instability is a straightforward consequence of the basic rules of the bifurcation theory, and, finally, dash-dotted lines pertain to soliton families destabilized by an intrinsic mode (in fact, they are transformed by the intrinsic instability into robust breathers, see below).

Figure 1 demonstrates that no solitons exist at very large values of λ. As it follows from Eqs. (8) and (7), with the decrease of λ symmetric soliton ψ_+ emerges, with zero amplitude, at

$$\lambda = \lambda_0 \equiv 1 + \sqrt{h^2 - \gamma^2} \approx 1.13 \tag{11}$$

(the particular numerical value is given for $h=0.42$ and $\gamma=0.40$). The soliton emerges as an unstable mode, due to the instability of the zero background. Direct simulations demonstrate that, in this regime, the instability transforms the soliton into a delocalized "turbulent" state (not shown here). With the further decrease of λ, the zero solution becomes stable at

$$\lambda = \lambda_{\text{stabil}} \equiv 1 - \sqrt{h^2 - \gamma^2} \approx 0.87, \tag{12}$$

in agreement with Eq. (5), and it can be verified that symmetric soliton ψ_+ becomes stable at the same point. Keeping to decrease λ, we encounter the supercritical SSB bifurcation of the pitchfork type, which destabilizes the symmetric soliton and simultaneously gives rise to a pair of stable asymmetric ones (below, the asymmetric solitons bifurcating from ψ_+ are sometimes referred to as A_+, with A standing for "asymmetric"). An exact result known for the standard DCF system [25] is that the SSB bifurcation in that model happens at $E=(8/\sqrt{3})\sqrt{\lambda}$. Using relation (10), this can be translated into the *exact* location of the bifurcation point in Fig. 1(b):

$$\lambda_{\text{bif}} = (3/5)(1 + \sqrt{h^2 - \gamma^2}) \approx 0.68. \tag{13}$$

As might be expected, unstable symmetric solitons past the bifurcation point show a clear trend to spontaneously rearrange themselves into stable asymmetric states, which is a straightforward manifestation of the SSB in the present setting. A typical example is shown in Fig. 2: a small asymmetric perturbation imposed onto an unstable symmetric soliton—actually, the multiplication of its ψ and ϕ components by 1.01 and 0.99, respectively—initiates its quick transformation into a stable asymmetric soliton.

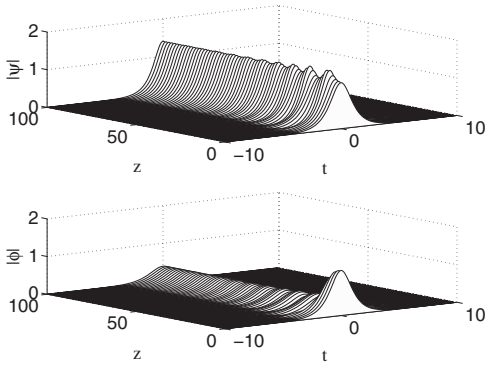

FIG. 2. A generic example of the spontaneous transformation of a slightly perturbed unstable symmetric soliton into a stable asymmetric one. Parameters are $h=0.42$, $\gamma=0.40$ (the same as in Fig. 1), and $\lambda=0.40$.

As λ approaches zero, the asymmetric solitons remain stable, in the present case, up to $\lambda=0$. A noteworthy finding is that the symmetric soliton, ψ_+, undergoes *restabilization* at

$$\lambda = \lambda_{\text{restab}} = \sqrt{h^2 - \gamma^2} \approx 0.13, \tag{14}$$

and remains stable up to point $\lambda=0$. Expression (14) for λ_{restab} can be obtained from the analysis of linearized equations for small perturbations around the symmetric soliton, similar to how expression (13) for λ_{bif} was found using the known results borrowed from the standard DCF model [25]. The restabilization of the symmetric soliton complies with the obvious fact that, at $\lambda=0$, the former asymmetric soliton corresponding to $\Theta=1$, and the symmetric one with $\Theta=0$ are tantamount to each other, as in this limit one gets back to the single-component model, which supports the single stable soliton, $\psi_+(t)$, see Eqs. (2). Actually, the restabilization is accounted for by an additional (*inverse pitchfork*) bifurcation at $\lambda=\lambda_{\text{restab}}$, which is also shown in Fig. 1. The pair of asymmetric solitons which merge into the symmetric one at this point are represented by a numerically found solution with a variable phase (alias with intrinsic *chirp*) that cannot be related to solitons of the DCF model by Eqs. (7). We designate this soliton family by symbol C, which stands for "chirped." A typical example of an unstable soliton of type C is displayed in Fig. 3.

The parameter region of $0<\lambda<\lambda_{\text{restab}}$ provides for a clear example of the bistability, as the symmetric soliton and two mirror-image variants of the asymmetric one are stable in this region. Actually, unstable branch C plays the role of a border (*separatrix*) between attraction basins of the two stable solutions (*attractors*), symmetric and asymmetric ones. The latter property is illustrated by Fig. 4, which shows that a numerically exact stationary solution of type C, if perturbed by $\{\psi_C(t),\phi_C(t)\}\rightarrow\{1.01\psi_C(t),0.99\phi_C(t)\}$, evolves into a stable strongly asymmetric soliton; if, instead, the perturbation is imposed by $\{\psi_C(t),\phi_C(t)\}\rightarrow\{0.99\psi_C(t),1.01\phi_C(t)\}$, it causes the spontaneous transformation of the initial C soliton into the stable symmetric one (which does not seem very different from its counterpart of type C, as the asymmetry of the latter mode is weak).

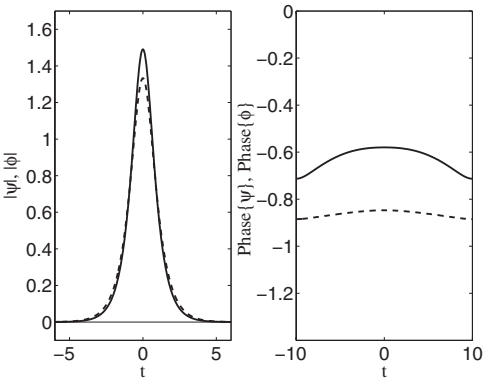

FIG. 3. An example of an unstable chirped soliton of type C, which accounts for the restabilization of the symmetric soliton at sufficiently small values of coupling constant λ. Parameters are $h=0.42$, $\gamma=0.40$ (the same as in Fig. 1), and $\lambda=0.06$.

C. Case 2: An unstable pitchfork bifurcation (strong parametric gain)

The bifurcation diagrams reported above are relevant to the case when, with the decrease of λ, the stabilization of the zero solution happens prior to the destabilization of the ψ_+ mode through the pitchfork bifurcation. In other words, this condition implies $\lambda_{\text{stabil}}>\lambda_{\text{bif}}$, or, as follows from Eqs. (12) and (13), $h^2<\gamma^2+1/16$.

If the parametric gain is stronger, i.e., $h^2>\gamma^2+1/16$, the SSB bifurcation happens on the unstable branch of the symmetric solutions, as shown in Fig. 5. Accordingly, the asymmetric solitons also emerge as unstable solutions. The further decrease of λ leads to the stabilization of the asymmetric solitons at point $\lambda=\lambda_{\text{stabil}}$, where the zero background becomes stable.

In fact, two different particular situations are possible in this case. If the gain is moderately strong, viz.,

$$\gamma^2 + 1/16 < h^2 < \gamma^2 + 1/4, \tag{15}$$

which is tantamount to $\lambda_{\text{restab}}<\lambda_{\text{stabil}}<\lambda_{\text{bif}}$ [see Eqs. (12) and (14)], the restabilization of the symmetric soliton occurs after the stabilization of the zero solution. In this case, the symmetric soliton remains unstable in interval $\lambda_{\text{restab}}<\lambda<\lambda_{\text{stabil}}$, as shown in Fig. 5(a). On the other hand, if the gain is still stronger, $h^2>\gamma^2+1/4$, Eqs. (12) and (14) formally predict $\lambda_{\text{stabil}}<\lambda_{\text{restab}}$. The actual meaning of this inequality is that the symmetric solitons become and remain stable immediately after the stabilization of the zero solution, i.e., in the entire region $0\leqslant\lambda<\lambda_{\text{stabil}}$, see Fig. 5(b). In this case, branch C is no longer linked by a bifurcation to the symmetric solitons. Instead, as shown in Fig. 5(b), branch C bifurcates into a bound complex of three asymmetric solitons, of type A_{-+-}, which means two asymmetric counterparts of solution ψ_-, and one of solution ψ_+ (recall A stands for "asymmetric"). This complex forms a completely unstable family, which is connected by an additional bifurcation to other unstable bound states of asymmetric solitons (not shown here). Actually, the present model supports a species of stable bound states of asymmetric solitons, which is considered in Sec. IV.

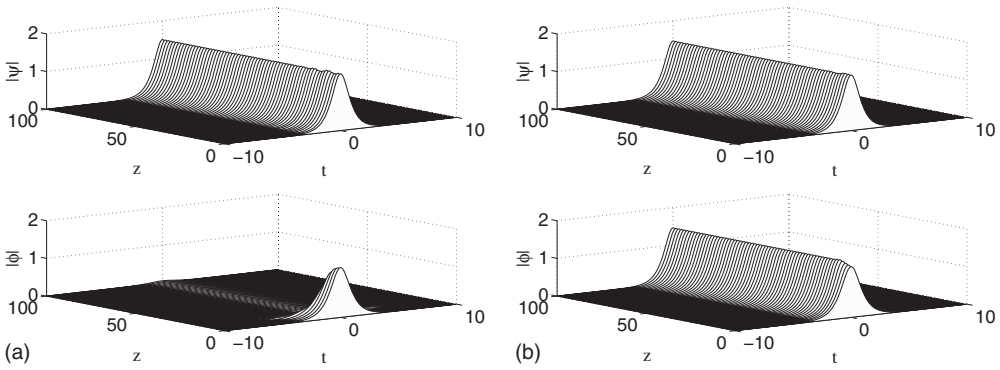

FIG. 4. Panels (a) and (b) display the evolution of an unstable weakly asymmetric chirped soliton of type C, which plays the role of the separatrix between attraction basins of the coexisting stable symmetric and strongly asymmetric solitons. Depending on the small initial perturbation, the unstable mode can transform itself into either of the two soliton attractors. Parameters are the same as in Fig. 3.

Note that the bistability is observed in both cases displayed in Fig. 5. Moreover, in Fig. 5(b), the entire region of the existence of stable solitons features the bistability.

D. Case 3: Instability in the limit of the vanishing coupling

The SSB diagrams displayed above in Figs. 1 and 5 do not exhaust all generic scenarios. Another case occurs when, after the restabilization at point (14), the symmetric soliton, ψ_+, is eventually destabilized at still smaller values of λ, as shown in Fig. 6. The critical value of λ at which this happens, $\lambda_{\text{destab}}^{(\text{symm})}$, can be found in a numerical form, from the stability analysis of the symmetric solitons against small perturbations, as shown below. In all such cases, the asymmetric solitons also get destabilized with the decrease of λ, although the respective critical value—for instance, $\lambda_{\text{destab}}^{(\text{asymm})}(h=0.50,\gamma=0.30)\approx 0.378$ in Fig. 6—is essentially larger than its counterpart for the symmetric soliton, which is

$$\lambda_{\text{destab}}^{(\text{symm})}(h=0.50,\gamma=0.30)\approx 0.118 \tag{16}$$

in Fig. 6. Thus we can identify a generic situation in which all solitons are unstable in the limit of the decoupled system ($\lambda=0$), but have a well-defined stability region at finite λ. Figure 6 also suggests that the bistability region is very small in this case, hence it may be useful to applications where the bistability should be avoided. On the other hand, it is relevant to mention that an intensive search of the parameter space has not revealed any example in which only the asymmetric soliton would be stable, while the family of the symmetric modes would be completely unstable.

As demonstrated in the next section, the destabilization of the symmetric soliton, ψ_+, in the region of $\lambda<\lambda_{\text{destab}}^{(\text{symm})}$ is accounted for by a pair of complex-conjugate eigenvalues in the spectrum of small perturbations. Accordingly, this *oscillatory* instability does not destroy the symmetric solitons, but rather transforms them into well-localized robust *breathers* which remain symmetric modes, see a typical example in Fig. 7. The breather remains a valid solution in the limit of $\lambda=0$, i.e., in the single-component model, in which it had been reported earlier [10] (in that work, it was also demonstrated that, deeper into the instability region, the breather may develop chaotic oscillations).

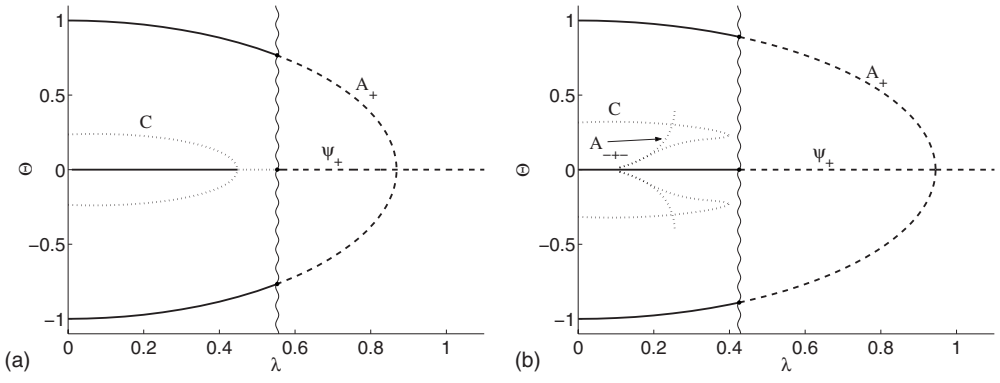

FIG. 5. Symmetry-breaking diagrams in the situation when the pitchfork bifurcation occurs before the stability of the zero solution is reached, cf. Fig. 1(b). Here and in the following figure, the stability border of the zero solution, corresponding to Eq. (12), is shown by the vertical wave line. (a) Case (15), when the restabilization of the symmetric soliton happens after the stabilization of the zero solution. (b) The case of $h^2>\gamma^2+1/4$, when the stabilization of the zero solution immediately makes the symmetric soliton stable too, while branch C of chirped asymmetric solutions is detached from the family of symmetric solitons, being instead linked to a family of unstable bound complexes A_{-+-}, see the text. In panel (b), although branches C and A_{-+-} merge with each other very close to $\Theta=0$, there is no bifurcation connecting them to the symmetric solitons. In this figure, the parameters are $\gamma=0.40$ and $h=0.60$ (a), or $h=0.70$ (b).

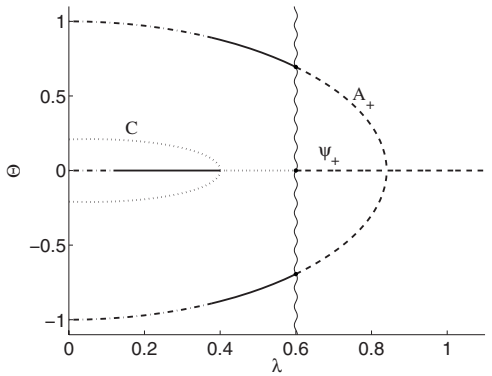

FIG. 6. The same as in Fig. 5, but for the case when additional bifurcations destabilize both symmetric and asymmetric solitons at small λ, making all the solitons unstable in the limit of the single-component system, $\lambda=0$. Parameters are $h=0.50$, $\gamma=0.30$.

The instability of asymmetric solitons in the region of $\lambda<\lambda_{\text{destab}}^{(\text{asymm})}$ is oscillatory too. It transforms these solitons into robust *asymmetric* breathers, as shown in Fig. 8.

III. STABILITY CHARTS FOR SYMMETRIC SOLITONS

As mentioned above, the full stability analysis for symmetric solitons $\psi_+(t)$, which are given by Eqs. (8) with $\sigma=+1$, can be performed rigorously. To this end, we take a perturbed solution in the form suggested by the analysis performed in the single-component model [10],

$$\psi(z,t)=\psi_+(t)+\delta e^{-i\theta_+-\gamma z}[f_\psi(z,t)+ig_\psi(z,t)],$$

$$\phi(z,t)=\psi_+(t)+\delta e^{-i\theta_+-\gamma z}[f_\phi(z,t)+ig_\phi(z,t)], \qquad (17)$$

where δ is an infinitesimal amplitude of the perturbation, and θ_+ is the same constant phase as in Eqs. (2). The substitution of these expressions in Eqs. (4) and linearization lead to a system of coupled equations for real functions $f_{\psi,\phi}(z,t)$ and $g_{\psi,\phi}(z,t)$. Solutions corresponding to a perturbation eigenmode with complex eigenvalue $\mu\equiv\nu+i\omega$ are then looked for in the following form:

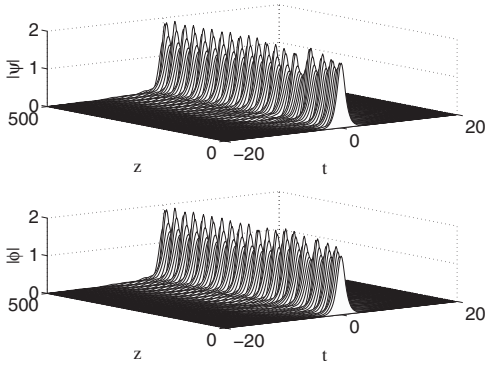

FIG. 7. A typical example of the formation of a robust symmetric breather from a symmetric soliton due to its oscillatory instability, at $h=0.50$, $\gamma=0.30$, and $\lambda=0.06$.

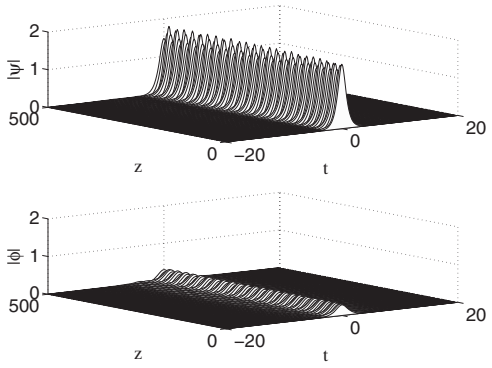

FIG. 8. An example of the formation of a robust asymmetric breather from an asymmetric soliton under the action of the oscillatory instability, at $h=0.50$, $\gamma=0.30$, and $\lambda=0.35$.

$$\{f_{\psi,\phi}(z,t),g_{\psi,\phi}(z,t)\}=e^{vZ}\,\mathrm{Re}\left[e^{i\omega Z}\left\{F_{\psi,\phi}(T),\frac{k}{\mu+\Gamma}G_{\psi,\phi}(T)\right\}\right], \qquad (18)$$

$$Z\equiv\frac{z}{(1-\lambda)+\sqrt{h^2-\gamma^2}},\quad T=\frac{t}{[(1-\lambda)+\sqrt{h^2-\gamma^2}]^{1/2}}, \qquad (19)$$

$$\Gamma\equiv\frac{\gamma}{(1-\lambda)+\sqrt{h^2-\gamma^2}},\quad k^2\equiv\mu^2-\Gamma^2. \qquad (20)$$

Substituting expressions (17) into underlying equations (4), performing the linearization, and making use of definitions (18)–(20), one can derive an eigenvalue problem based on the system of four equations for functions $F_{\psi,\phi}(T)$ and $G_{\psi,\phi}(T)$ with zero boundary conditions at $T\to\pm\infty$:

$$kF_{\psi,\phi}=\hat{L}_0G_{\psi,\phi}-\Lambda G_{\phi,\psi},\quad -kG_{\psi,\phi}=\hat{L}_1F_{\psi,\phi}-\Lambda F_{\phi,\psi}. \qquad (21)$$

Here we have additionally defined

$$\Lambda\equiv\frac{\lambda}{(1-\lambda)+\sqrt{h^2-\gamma^2}},\quad \varepsilon\equiv\frac{2\sqrt{h^2-\gamma^2}}{(1-\lambda)+\sqrt{h^2-\gamma^2}},$$

$$\hat{L}_0\equiv-\frac{1}{2}\frac{d^2}{dT^2}+1+\Lambda-\varepsilon-2\,\mathrm{sech}^2(\sqrt{2}T),$$

$$\hat{L}_1\equiv-\frac{1}{2}\frac{d^2}{dT^2}+1+\Lambda-6\,\mathrm{sech}^2(\sqrt{2}T). \qquad (22)$$

The linear eigenvalue problem based on Eqs. (21) was solved by means of the standard method, which uses the finite-difference approximation to reduce the problem to dealing with a large-size matrix. The resulting eigenvalues are displayed in Fig. 9, in the form of real and imaginary parts of quadratic eigenvalue k versus aggregate parameter ε [these are defined as per Eqs. (20) and (22)], for several fixed values of coupling constant λ. Actually, Eqs. (21) give rise to two branches of $k(\varepsilon)$: one marked by the respective values of λ in Fig. 9, and the other coinciding, at all values of λ, with

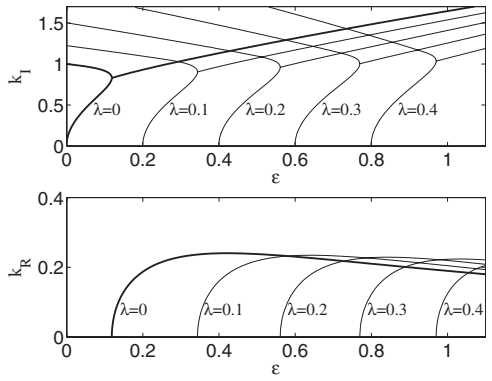

FIG. 9. Imaginary and real parts of eigenvalue $k \equiv k_R + ik_I$ versus parameter ε, which are defined as per Eqs. (20) and (22).

the solution for $\lambda=0$ (therefore k becomes a double eigenvalue in the limit of $\lambda \to 0$). Branch $k(\varepsilon)$ for $\lambda=0$ displayed in Fig. 9 is exactly the same as its counterpart which had been found, in the framework of the single-component model, in Ref. [10].

Straightforward manipulations with the above definitions demonstrate that the stability region of the symmetric solitons can be represented in the following form, in terms of complex eigenvalue k displayed in Fig. 9:

$$\gamma \geqslant \gamma_{\rm cr} \equiv \frac{2(1-\lambda)}{(2-\varepsilon)} \frac{k_I k_R}{\sqrt{k_I^2 - k_R^2}}. \tag{23}$$

Substituting numerical data for k in Eq. (23), and combining it with condition $\lambda < \lambda_{\rm stabil}$ necessary for the stability of the zero background [see Eq. (12)], we identify a full stability region for the symmetric solitons in the plane of the loss and gain coefficients, (γ, h). For several fixed values of λ, the stability region is displayed in Fig. 10. All panels in this figure include, for the sake of comparison, borders of the stability domain (shown by chains of empty circles) that can be found, for $\lambda=0$, in the single-component model, as originally done in Refs. [10,11].

The comparison of expressions (12)–(14), where the symmetric solitons undergo, respectively, the stabilization of their background, destabilization through the SSB bifurcation, and restabilization through the inverse bifurcation (which also gives rise to chirped states C), readily demonstrates that, in the region of $\lambda < 1/2$ [see Figs. 10(a)–10(c)], all stable symmetric solitons are actually *restabilized* ones. In the intermediate interval $1/2 < \lambda < 3/5$, the symmetric solitons cannot be stable, while in the region of $\lambda > 3/5$ [to which Figs. 10(d)–10(f) belong] those symmetric solitons are stable which have undergone the stabilization of the background but did not yet hit the bifurcation point. Moreover, in interval $3/5 < \lambda < 3/4$ curve VI in Figs. 10(d) and 10(e), which is the locus of bifurcation points (13), determines the upper border of the stability area, while, at $\lambda > 3/4$, the same role is played by curve II [see Fig. 10(f)], which accounts for the stabilization of the zero background, according to Eq. (12).

IV. TWO-SOLITON BOUND STATES

Unlike fundamental solitons, which follow the pattern of the NLS soliton solutions, bound states of two or several pulses cannot exist with constant phases θ [cf. Eq. (6)], as all solutions with θ=const automatically reduce to fundamental solitons. Several families of multipulse complexes with $\theta \neq$ const have been previously found in the single-component parametrically driven NLS equation [12]. The single family a part of which is stable represents bound states of two fundamental solitons of type ψ_+, see Eq. (2). This species of the bound states is designated here as ψ_{++}. It emerges from a pair of infinitely separated fundamental solitons, (ψ_+, ψ_+), and keeps a two-peak shape as long as it remains stable (unstable portions of the family are connected to branches of three-peak unstable modes). The point at which complex ψ_{++} emerges from the infinitely separated pair in the single-component model is $q=\sqrt{h^2-\gamma^2}$ [12]. In the present notation, this point is $\lambda = 1-\sqrt{h^2-\gamma^2} \equiv \lambda_{\rm stabil}$, i.e., it coincides with point (12) at which the zero solution becomes stable.

As well as the fundamental (single-peak) solitons, in the system of coupled equations (4) the family of dual-peak symmetric states ψ_{++} undergoes the SSB, via a bifurcation that gives rise to asymmetric dual-peak bound states. In line with the notation used above, these asymmetric complexes are denoted A_{++} (recall A stands for asymmetric). We stress that the symmetry is broken between their ψ and ϕ components, while the spatial symmetry between two peaks of the solutions does not change, see Fig. 11.

States A_{++} emerge, from a pair of infinitely separated asymmetric fundamental solitons, (A_+, A_+), at exactly the same point, $\lambda=\lambda_{\rm stabil}$ [see Eq. (12)], where the symmetric bound state, ψ_{++}, originates from the infinitely separated pair of (ψ_+, ψ_+), as said above. Further, the asymmetric dual-peak bound state A_{++} really exists if it emerges at the above-mentioned point, $\lambda=\lambda_{\rm stabil}$, *later* (i.e., at smaller λ) than the fundamental asymmetric soliton, A_+, bifurcates, at $\lambda=\lambda_{\rm bif}$, from its symmetric counterpart ψ_+ (this conclusion is well-corroborated by numerical findings). In other words, the existence condition for asymmetric complex A_{++} is $\lambda_{\rm stabil} < \lambda_{\rm bif}$, or, as follows from Eqs. (13) and (12), $h^2 > \gamma^2 + 1/16$. It is worthy to note that this is the same condition which selects the bifurcation diagrams for the fundamental solitons in the form shown in Fig. 5, see Eq. (15). On the other hand, in the case of $h^2 < \gamma^2 + 1/16$ [which is, simultaneously, the condition that selects the single-soliton bifurcation diagrams displayed in Fig. 1(b)], asymmetric bound states A_{++} do not exist.

A set of generic diagrams which demonstrates the transition between the symmetric and asymmetric two-soliton complexes, and shows the stability of both types of the double-peak solutions, is presented in Fig. 12. The situation displayed in Fig. 12(a) pertains to the above-mentioned case of $h^2 < \gamma^2 + 1/16$, where the asymmetric two-soliton bound states do not exist. The other panels in Fig. 12 correspond to $h^2 > \gamma^2 + 1/16$, hence the branch of asymmetric complexes A_{++} exists in the respective cases. This branch connects the SSB bifurcation point, where A_{++} splits off from its symmetric counterpart ψ_{++}, and $\lambda=\lambda_{\rm stabil}$, where, as mentioned

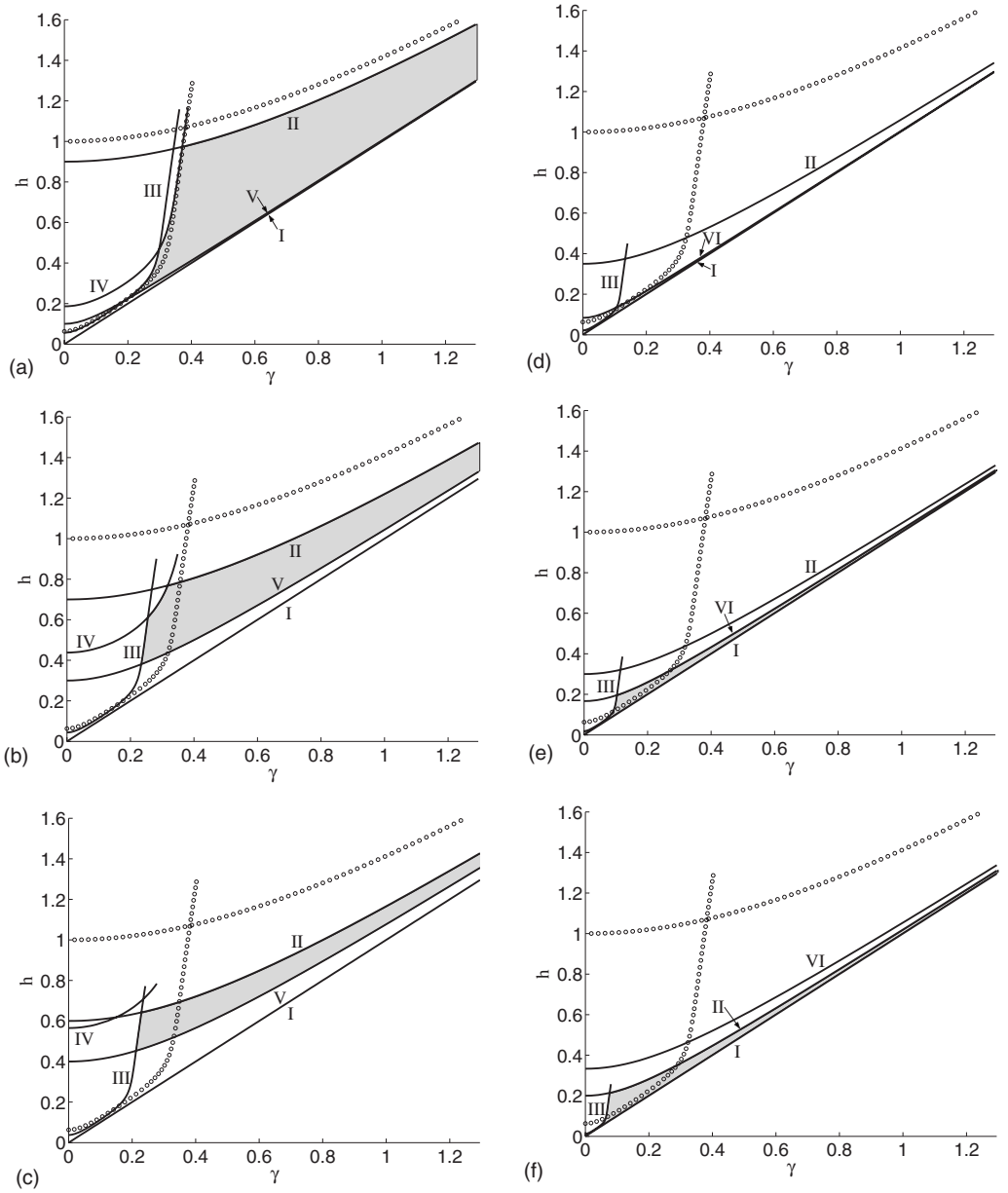

FIG. 10. The stability region (shaded) for symmetric solitons, whose analytical form is given by Eq. (8) with $\sigma=+1$, in the plane of (γ,h), for a fixed value of coupling constant: (a) $\lambda=0.10$; (b) $\lambda=0.30$; (c) $\lambda=0.40$; (d) $\lambda=0.65$; (e) $\lambda=0.70$; and (f) $\lambda=0.80$ (in the interval of $0.50<\lambda<0.60$, there are no stable symmetric solitons, see the text). In each panel, border I represents the existence condition for the solitons, $h\geqslant\gamma$. Curve II denotes the stability border for the zero solution, $\lambda\leqslant\lambda_{\text{stab}}$, as per Eq. (12). Border lines III and IV are determined, in the numerical form, by Eq. (23), as conditions for the stability against localized perturbations. Finally, curves V and VI correspond, respectively, to the restabilization border, as given by Eq. (14), and the locus of the bifurcation points, as per Eq. (13). Chains of circles indicate borders of the stability area in the single-component model, with $\lambda=0$.

above, A_{++} emerges from the pair of infinitely separated fundamental asymmetric solitons, (A_+,A_+). The relation of bound states A_{++} and ψ_{++} to the respective pairs of infinitely separated fundamental solitons is made clear by the reference lines in Fig. 12, which are depicted by chains of empty squares and indicate families of such noninteracting pairs. Further, in Figs. 12(b) and 12(c) one naturally observes that the A_{++} family is stable past the bifurcation point. Simultaneously, the bifurcation, as expected, destabilizes the symmetric bound states, ψ_{++}.

In addition to that, Fig. 12(d) demonstrates that there is a parameter region where the branches of the symmetric and antisymmetric complexes, ψ_{++} and A_{++}, are completely independent, without being linked by the bifurcation. In this situation, the family of symmetric bound states ψ_{++} is completely unstable, while a part of the branch of A_{++} remains stable. In fact, in Figs. 12(a)–12(d) the unstable portion of the ψ_{++} branch terminates at a point where it is linked to another family of unstable symmetric complexes, which gradually develop a three-soliton shape of type ψ_{-+-} (the

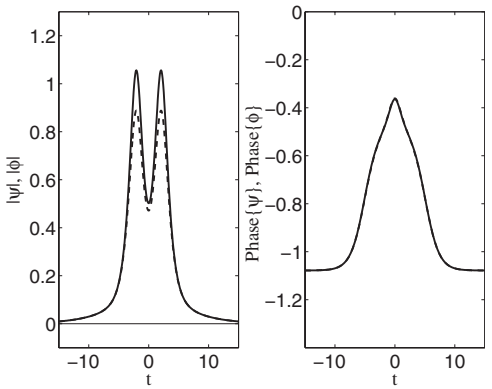

FIG. 11. A typical example of a stable double-peak complex featuring the asymmetry between its two components, $\psi(t)$ and $\phi(t)$, while each component maintains the spatially symmetric profile. The phases of the ψ and ϕ components, shown in the right-hand panel, are almost identical. Parameters are $h=0.48$, $\gamma=0.40$, and $\lambda=0.71$.

same was concluded in Ref. [12], although it appears there was an error in describing the transition from ψ_{++} to ψ_{-+-}). Similarly, in Fig. 12(d) the unstable portion of branch A_{++} is linked to a family of unstable bound states designated as $\psi_- A_+ \psi_-$. These may be regarded as complexes composed of two (almost) symmetric unstable fundamental solitons ψ_-, with the asymmetric fundamental soliton, A_+, sandwiched between them.

Lastly, it is relevant to mention that our analysis of the stationary version of Eqs. (4) has revealed several other types of multipulse complexes, including those featuring two peaks in one component and three in the other, or, respectively, one and two peaks. These states originate from the unstable fundamental symmetric soliton, ψ_-, see Eq. (2), or from antisymmetric ones, see Eqs. (8), and demonstrate intricate patterns of bifurcations. However, they all are unstable, therefore we do not report them in detail here.

V. CONCLUSION

In this work, we have introduced a model describing a dual-core nonlinear optical fiber, or a planar waveguide, in which the loss is compensated by the parametric gain symmetrically applied to both cores. This fiber or waveguide may be the main element of a laser featuring controllable bistability and switching. The same model applies to the description of parallel ferromagnetic films, in which the parametric gain is provided by an external field. The main subject of the analysis was the spontaneous symmetry breaking (SSB) of fundamental and multiple solitary pulses in this setting. While the SSB was studied in detail in conservative models, it remains largely unexplored in linearly coupled dissipative systems.

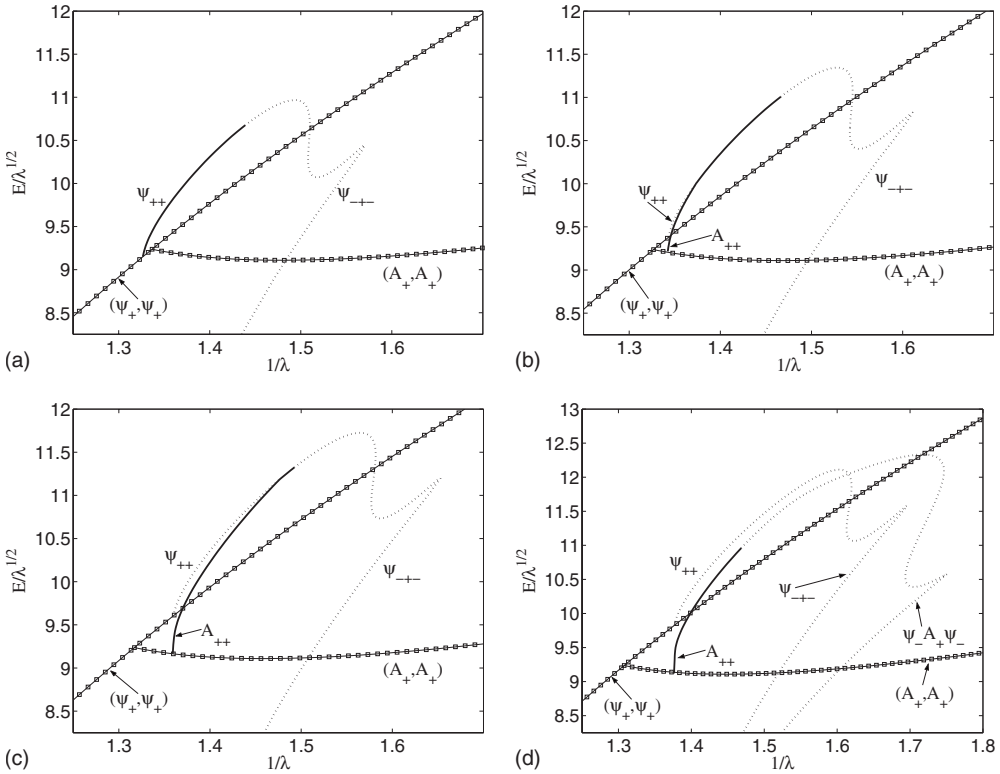

FIG. 12. The bifurcation diagrams, similar to that displayed in Fig. 1(a), but for families of symmetric and asymmetric two-soliton complexes, ψ_{++} and A_{++}. Stable and unstable portions of the families are represented by continuous and dotted segments of the curves. For the sake of comparison, the chains of squares represent the states formed by pairs of infinitely separated symmetric and asymmetric solitons, (ψ_+,ψ_+) and (A_+,A_+). Parameters are $\gamma=0.40$ and $h=0.470$ (a), 0.475 (b), 0.480 (c), and 0.485 (d). In case (a), asymmetric bound states A_{++} do not exist. In case (d), the families of the symmetric and asymmetric complexes, ψ_{++} and A_{++}, are disconnected, the intersection between the respective curves being spurious (it does not imply any bifurcation).

The analysis reported in the paper reveals three distinct SSB scenarios for fundamental solitons. Unlike what was previously found in the standard model of the dual-core fiber (DCF), in the present system the SSB bifurcation is supercritical, and it leads to a vast bistability region in the system's parameter space. Noteworthy findings are the restabilization (through the additional inverse pitchfork bifurcation, involving the pair of asymmetric chirped modes, of the "C" type) of the symmetric soliton that was destabilized by the SSB bifurcation, and the discovery of a generic situation in which all stationary solitons are unstable in the decoupled (single-component) system, but they (both symmetric and asymmetric ones) may be stable—or, actually, bistable—in the presence of the linear coupling. In the latter case, the unstable symmetric and asymmetric solitons in the weakly coupled system are replaced by robust breathers that maintain their symmetry, or the lack thereof, respectively.

The stability of the asymmetric states was identified by means of systematic simulations, while for symmetric and antisymmetric modes the stability has also been verified through the computation of eigenvalues for small perturbations. As a result, full stability charts for the symmetric solitons have been plotted, and the difference from their counterpart in the single-component model was highlighted. As for antisymmetric states, they all are unstable.

We have also investigated multisoliton bound states and found the SSB bifurcation of two-soliton complexes that gives rise to stable asymmetric complexes; they are asymmetric as concerns the inequality between the two components, while the spatial symmetry between the two peaks remains intact. The families of symmetric and asymmetric bound states may be unlinked when the SSB bifurcation that connects them disappears. In the latter situation, the family of the symmetric double-peak complexes is completely unstable, while a part of the branch of the asymmetric complexes remains stable.

This work can be extended in several directions. On the one hand, it may be relevant to add the nonlinear coupling between the two components, mediated by the cross-phase-modulation, and analyze its effects on the SSB bifurcations and stability of various localized states in the dual-core system with a considerable overlap between the single-core modal profiles (in terms of matter-wave models, a similar analysis was reported in Ref. [36]). On the other hand, it may also be interesting to study moving solitons and collisions between them in the lossless setting, with $\gamma=0$, which was done for the single-component model in Ref. [37]. Moreover, in Ref. [38] it was demonstrated that specific moving complexes of bound solitons, which feature zero total momentum at nonzero velocity, are possible even in the presence of the loss. It might be quite interesting to look for moving complexes in the coupled system too.

[1] I. S. Aranson and L. Kramer, Rev. Mod. Phys. **74**, 99 (2002); B. A. Malomed, in *Encyclopedia of Nonlinear Science*, edited by A. Scott (Routledge, New York, 2005), p. 157.

[2] G. P. Agrawal, *Fiber-Optic Communication Systems* (Wiley, New York, 1997); E. Iannone, F. Matera, A. Mecozzi, and M. Settembre, *Nonlinear Optical Communication Networks* (Wiley, New York, 1998).

[3] J. D. Moores, Opt. Commun. **96**, 65 (1993); C. J. Chen, P. K. A. Wai, and C. R. Menyuk, Opt. Lett. **19**, 198 (1994); F. X. Kartner, I. D. Jung, and U. Keller, IEEE J. Sel. Top. Quantum Electron. **2**, 540 (1996); N. Akhmediev, J. M. Soto-Crespo, and G. Town, Phys. Rev. E **63**, 056602 (2001).

[4] B. A. Malomed, Physica D **29**, 155 (1987); S. Fauve and O. Thual, Phys. Rev. Lett. **64**, 282 (1990); V. Hakim, P. Jakobsen, and Y. Pomeau, Europhys. Lett. **11**, 19 (1990); B. A. Malomed and A. A. Nepomnyashchy, Phys. Rev. A **42**, 6009 (1990).

[5] B. A. Malomed and H. G. Winful, Phys. Rev. E **53**, 5365 (1996); J. Atai and B. A. Malomed, *ibid.* **54**, 4371 (1996).

[6] J. Atai and B. A. Malomed, Phys. Lett. A **246**, 412 (1998).

[7] J. Atai and B. A. Malomed, Phys. Lett. A **244**, 551 (1998).

[8] H. Sakaguchi and B. A. Malomed, Physica D **147**, 273 (2000).

[9] B. A. Malomed, Chaos **17**, 037117 (2007).

[10] I. V. Barashenkov, M. M. Bogdan, and V. I. Korobov, Europhys. Lett. **15**, 113 (1991).

[11] M. Bondila, I. V. Barashenkov, and M. M. Bogdan, Physica D **87**, 314 (1995); S. Longhi, G. Steinmeyer, and W. S. Wong, J. Opt. Soc. Am. B **14**, 2167 (1997); N. V. Alexeeva, I. V. Barashenkov, and D. E. Pelinovsky, Nonlinearity **12**, 103 (1999); V. S. Shchesnovich and I. V. Barashenkov, Physica D **164**, 83 (2002).

[12] I. V. Barashenkov, Yu. S. Smirnov, and N. V. Alexeeva, Phys. Rev. E **57**, 2350 (1998); I. V. Barashenkov and E. V. Zemlyanaya, Phys. Rev. Lett. **83**, 2568 (1999).

[13] H. P. Yuen, Phys. Rev. A **13**, 2226 (1976); H. P. Yuen, Opt. Lett. **12**, 789 (1987); **17**, 73 (1992); R. Loudon, IEEE J. Quantum Electron. **21**, 766 (1985).

[14] J. N. Kutz, W. L. Kath, R.-D. Li, and P. Kumar, Opt. Lett. **18**, 802 (1993); C. G. Goedde, W. L. Kath, and P. Kumar, *ibid.* **19**, 2077 (1994); R. D. Li, P. Kumar, and W. L. Kath, J. Lightwave Technol. **12**, 541 (1994); J. N. Kutz, C. V. Hile, W. L. Kath, R.-D. Li, and P. Kumar, J. Opt. Soc. Am. B **11**, 2112 (1994); I. H. Deutsch and I. Abram, J. Opt. Soc. Am. B **11**, 2303 (1994); S. Longhi, Opt. Lett. **20**, 1628 (1995); J. Mod. Opt. **43**, 1089 (1996); K. Staliunas, *ibid.* **42**, 1261 (1995); G.-L. Oppo, A. J. Scroggie, and W. J. Firth, Phys. Rev. E **63**, 066209 (2001).

[15] S. Longhi, Opt. Lett. **21**, 860 (1996); , Europhys. Lett. **37**, 257 (1997); Opt. Commun. **149**, 335 (1998).

[16] J. Corones, Phys. Rev. B **16**, 1763 (1977); B. A. Ivanov, A. M. Kosevich, and I. V. Manzhos, Solid State Commun. **34**, 417 (1980).

[17] A. M. Kosevich, B. A. Ivanov, and A. S. Kovalev, Phys. Rep. **194**, 117 (1990).

[18] P. Coullet, J. Lega, and Y. Pomeau, Europhys. Lett. **15**, 221 (1991); I. V. Barashenkov, S. R. Woodford, and E. V. Zemlyanaya, Phys. Rev. Lett. **90**, 054103 (2003).

[19] H. Sakaguchi and B. A. Malomed, Physica D **167**, 123 (2002); J. Phys. Soc. Jpn. **72**, 1360 (2003); I. V. Barashenkov, S. Cross, and B. A. Malomed, Phys. Rev. E **68**, 056605 (2003).

[20] T. Frisch, S. Rica, P. Coullet, and J. M. Gilli, Phys. Rev. Lett. **72**, 1471 (1994); T. Frisch, Physica D **84**, 601 (1995).
[21] J. W. Miles, J. Fluid Mech. **148**, 451 (1984); C. Elphick and E. Meron, Phys. Rev. A **40**, 3226 (1989); W. Zhang and J. Viñals, Phys. Rev. Lett. **74**, 690 (1995); X. Wang and R. Wei, Phys. Rev. E **57**, 2405 (1998).
[22] S. V. Kiyashko, L. N. Korzinov, M. I. Rabinovich, and L. S. Tsimring, Phys. Rev. E **54**, 5037 (1996); L. S. Tsimring and I. S. Aranson, Phys. Rev. Lett. **79**, 213 (1997).
[23] P. Coullet, Phys. Rev. Lett. **56**, 724 (1986).
[24] A. W. Snyder, D. J. Mitchell, L. Poladian, D. R. Rowland, and Y. Chen, J. Opt. Soc. Am. B **8**, 2102 (1991).
[25] E. M. Wright, G. I. Stegeman, and S. Wabnitz, Phys. Rev. A **40**, 4455 (1989).
[26] C. Paré and M. Fłorjańczyk, Phys. Rev. A **41**, 6287 (1990).
[27] N. N. Akhmediev and A. Ankiewicz, Phys. Rev. Lett. **70**, 2395 (1993); J. M. Soto-Crespo and N. N. Akhmediev, Phys. Rev. E **48**, 4710 (1993); N. N. Akhmediev and J. M. Soto-Crespo, *ibid.* **49**, 4519 (1994).
[28] P. L. Chu, B. A. Malomed, and G. D. Peng, J. Opt. Soc. Am. B **10**, 1379 (1993); B. A. Malomed, I. M. Skinner, P. L. Chu, and G. D. Peng, Phys. Rev. E **53**, 4084 (1996).
[29] W. C. K. Mak, B. A. Malomed, and P. L. Chu, J. Opt. Soc. Am. B **15**, 1685 (1998); Phys. Rev. E **69**, 066610 (2004); A. Gubeskys and B. A. Malomed, Eur. Phys. J. D **28**, 283 (2004); Y. J. Tsofe and B. A. Malomed, Phys. Rev. E **75**, 056603 (2007).
[30] M. Jensen, IEEE Trans. Microwave Theory Tech. **MTT-30**, 1568 (1982); A. A. Maier, Sov. J. Quantum Electron. **12**, 1490 (1982).
[31] D. D. Gusovskii, E. M. Dianov, A. A. Maier, V. B. Nestruev, V. V. Osiko, A. M. Prokhorov, K. Yu. Sitarskii, and I. A. Shcherbakov, Sov. J. Quantum Electron. **17**, 724 (1987); S. R. Friberg, A. M. Weiner, Y. Silberberg, B. G. Sfez, and P. S. Smith, Opt. Lett. **13**, 904 (1988).
[32] A. Sigler and B. A. Malomed, Physica D **212**, 305 (2005); A. Sigler, B. A. Malomed, and D. V. Skryabin, Phys. Rev. E **74**, 066604 (2006).
[33] B. A. Malomed, in *Progress in Optics*, edited by E. Wolf (North-Holland, Amsterdam, 2002), Vol. 43, p. 71.
[34] F. Kh. Abdullaev, R. M. Abrarov, and S. A. Darmanyan, Opt. Lett. **14**, 131 (1989).
[35] Q. Chang, E. Jia, and W. Sun, J. Comput. Phys. **148**, 397 (1999).
[36] M. I. Merhasin, B. A. Malomed, and R. Driben, J. Phys. B **38**, 877 (2005); S. K. Adhikari and B. A. Malomed, Phys. Rev. A **74**, 053620 (2006).
[37] I. V. Barashenkov, E. V. Zemlyanaya, and M. Bär, Phys. Rev. E **64**, 016603 (2001).
[38] E. V. Zemlyanaya and I. V. Barashenkov, SIAM J. Appl. Math. **64**, 800 (2004).